https://doi.org/10.5194/egusphere-2025-5296
Preprint. Discussion started: 21 December 2025

Underestimated Future Arctic Ocean Warming due to Unresolved Marine Heatwaves at Low Resolution

Ruijian Gou[1,2], Yaocheng Deng[3], Yingzhe Cui[3], Qi Shu[4], Hong Wang[1], Shengpeng Wang[1], Lixin Wu[1,3], Gerrit Lohmann[2,5]

[1]Laoshan National Laboratory, Qingdao, China.
[2]Alfred Wegener Institute, Bremerhaven, Germany.
[3]Frontiers Science Center for Deep Ocean Multispheres and Earth System and Key Laboratory of Physical Oceanography, Ocean University of China, Qingdao, China
[4]First Institute of Oceanography, MNR, Qingdao, China.
[5]University of Bremen, Bremen, Germany.

Correspondence to: Ruijian Gou (rgou@foxmail.com)

Abstract. The Arctic Ocean is projected to warm twice more than the global mean in a warming 21st century, following increased solar heat input due to sea ice decrease. Here we find that this increase in solar heat input is larger in a higher-resolution climate model compared to a low-resolution one. This is due to the impacts of Arctic marine heatwaves (MHWs), known as episodes of extreme ocean warming. The explicit consideration of MHWs, which are stronger and more realistic in higher-resolution models, increases melting of sea ice and thus solar heat input, thereby reinforcing the long-term Arctic Ocean warming. A positive feedback is identified between stronger MHWs and larger Arctic Ocean warming. We emphasize that Arctic Ocean warming is underestimated by the current generation of climate models, which generally have a too low spatial resolution to resolve Arctic MHWs. We conclude that future eddy- and storm-resolving models will provide a new perspective on the Earth system's response to past and future climate and environmental extremes.

1 Introduction

As a result of anthropogenic global warming, the Arctic surface air has warmed four times faster than the rest of the Earth(Rantanen et al., 2022), a phenomenon known as Arctic amplification(Serreze, Barrett, Stroeve, Kindig, & Holland, 2009) that has severe global climate impacts(Judah Cohen et al., 2014; J. Cohen et al., 2020). The drivers of Arctic amplification(Taylor, 2018) are mainly the local radiative feedbacks and remote forcing mechanisms. Local radiative feedbacks include ice-albedo feedback(Screen & Simmonds, 2010), lapse rate feedback and Planck feedback(Beer & Eisenman, 2022; Pithan & Mauritsen, 2014; Stuecker et al., 2018), water vapor feedback(Graversen & Wang, 2009), cloud feedbacks(Mitchell, Senior, & Ingram, 1989; Morrison, Kay, Frey, Chepfer, & Guzman, 2019). Remote forcing mechanisms include changes in atmosphere(Manabe & Wetherald, 1980) and ocean heat transports(Shu et al., 2022; Xu et al., 2024). There is a wide debate about the relative contributions of each mechanism(Previdi, Smith, & Polvani, 2021) leading to Arctic amplification. Among these mechanisms, a major one is the ice-albedo feedback(Goosse et al., 2018; Previdi et al.,

https://doi.org/10.5194/egusphere-2025-5296
Preprint. Discussion started: 21 December 2025

2021): since sea ice has higher albedo than sea water, thus with sea ice melting, ocean receives more solar radiation, and subsequent upward turbulent heat fluxes in later fall and winter amplify the atmospheric Arctic warming(Screen & Simmonds, 2010).

The underlying Arctic Ocean could influence the climate via interactions with atmosphere and sea ice. Based on rather limited observations, it has also warmed significantly, at least in some regions(Polyakov et al., 2020; Polyakov et al., 2017; Watelet et al., 2020). Low-resolution models from CMIP6 ensemble has projected an Arctic Ocean warming at a rate more than twice the global mean rate, a phenomenon named as Arctic Ocean amplification(Shu et al., 2022). Ocean heat transport is indicated to be a main driver of Arctic Ocean amplification(Shu et al., 2022). In high-resolution model version, enhanced transport by resolved ocean currents at Bering Strait leads to even stronger warming in the Arctic(Xu et al., 2024). High-resolution climate models also simulate climate extremes more accurately than low-resolution models(Contzen, Dickhaus, & Lohmann, 2022). With the retreat of sea ice, the Arctic Ocean would show more fluctuations and thus climate extremes due to air-sea interactions. For example, due to the increasing open-ocean area, Arctic marine heatwaves (MHWs), known as extreme warming episodes(Hobday et al., 2016), have become more intense, persistent, frequent in recent decades(Hu, Zhang, & Qian, 2020). Although simulations of MHWs still show a bias toward fewer and weaker MHWs(Pilo, Holbrook, Kiss, & Hogg, 2019), the gap between model and observation reduces with increasing model resolution(Guo et al., 2022; Hayashida, Matear, Strutton, & Zhang, 2020; Pilo et al., 2019), as intrinsic variability is increased by the small-scale air-sea interactions(Holbrook et al., 2019) and ocean eddies(Bian et al., 2023; Gruber, Boyd, Frölicher, & Vogt, 2021).

With a cutting-edge eddy-permitting (abbreviated as CESM-HR) model and low-resolution analogue version (abbreviated as CESM-LR) (Section 2.1), we study the linkage between long-term Arctic Ocean warming and short-term MHWs. The MHWs simulated in CESM-HR are of higher intensity and frequency than CESM-LR and low-resolution models from CMIP5 ensemble, with closer magnitudes to observational MHWs(Guo et al., 2022). Therefore, we ask whether future Arctic warming depends on model resolution when accounting for better-resolved MHWs in high-resolution models.

2 Data and Methods

2.1 Climate models for studying the mechanism

The high-resolution climate model and the low-resolution analogue version are based on CESM 1.3(Meehl et al., 2019). The high-resolution version has a nominal horizontal resolution of 0.1° in the ocean and sea ice components and 0.25° in the atmosphere and land components. The low-resolution version has a nominal horizontal resolution of 1° in the ocean and atmosphere components, which is consistent with most climate models of current generation. The oceanic eddies are parameterized in the low-resolution version. Both versions start from a pre-industrial control run and then are run from 1850 to 2100. CMIP5 historical forcing is used for 1850-2005 and representative concentration pathway 8.5 (RCP8.5) is used for 2006-2100(Masson-Delmotte et al., 2021). RCP8.5 is a high CO_2 emission scenario, with an additional radiative forcing of

https://doi.org/10.5194/egusphere-2025-5296
Preprint. Discussion started: 21 December 2025

8.5 W/m² by the year 2100. The spin-up time for the 1850-2100 run is 250 years, with climate forcings fixed to 1850 conditions. The detailed set up of the models can be found in an overview paper(Chang et al., 2020).

2.2 Observation-based dataset

The daily SST data from Optimum Interpolation Sea Surface Temperature (OISST)(Reynolds et al., 2007), provided by the National Oceanic and Atmospheric Administration, is used for calculating the observational MHW. The horizontal resolution is 1/4° and the time span is from 1 January 1988 to 31 December 2022. This dataset is a combination of observations from ships, satellites and buoys and is often used for MHW analyses(Hobday et al., 2016).

2.3 HighResMIP

The name and resolution of models from HighResMIP(Haarsma et al., 2016) are summarized in Table. S1. The chosen time period of each model is 1950-2050, with 1950-2014 and 2015-2050 each applied with historical forcing and Shared Socioeconomic Pathway 5-8.5 (SSP5-8.5, similar as RCP8.5 but combined with socioeconomic reasons)(Masson-Delmotte et al., 2021). For the comparison of each model between high-resolution and low-resolution versions, the same single ensemble numbers are selected. The ensemble numbers for CNRM-CM6-1 and EC-Earth3P are r1i1p1f2 and r1i1p2f1 respectively, and the ensemble number for the other models is r1i1p1f1. The ECMWF and AWI models are not included because of the lack of highres-future scenario (2015-2050).

The reason for not applying the same metric of period selection as CESM for HighResMIP models is that the large model spread in SIC across HighResMIP (e.g., Fig. 10a in Ref. (Selivanova, Iovino, & Cocetta, 2024)) make it inapplicable for constraining a same SIC change for all models. Fixing the time range from 1950 to 2050 provides the same climate background for all the models. It instead shows the dependence of Arctic Ocean warming on model resolution and indicates the stronger Arctic Ocean warming in higher-resolution models.

2.4 Marine heatwaves

The definition of MHW follows the benchmark in the MHW field(Frölicher, Fischer, & Gruber, 2018; Hobday et al., 2016). The MHW is defined as an extreme warming event lasting for at least 5 days during which the SST exceeds a threshold of 90%. Two MHWs with a gap no longer than two days are considered as a single continuous MHW. For the model, the threshold of each day is calculated with the daily SST of 11-day windows (the day is centered) within a 31-year moving baseline (the year of the day is centered) so that the 90% threshold is based on 341 daily SST values. A 31-day running mean is then applied for smoothing the thresholds. The moving baseline is suitable for the future warming scenario as it excludes the MHWs caused by the background warming instead of the change in extreme variability(Oliver et al., 2021). Since the calculation is based on the daily SST from 1950 to 2100, the results according to the moving baseline exclude the first and last 15 years of 1950-2100. The threshold for the observational dataset is the same, except for the baseline which covers the whole period (1982-2022), as the timespan is too short to make moving baselines. For MHW property, the cumulative

https://doi.org/10.5194/egusphere-2025-5296
Preprint. Discussion started: 21 December 2025

intensity is the integral of SST anomaly above the threshold over MHW duration. The annual-mean cumulative intensity is the average of annual cumulative intensity.

2.5 Ocean heat budget

The ocean heat budget is defined as

$$\underbrace{\left\langle \int_{-h}^{0} \rho_0 c_p \frac{\partial T}{\partial t} dz \right\rangle}_{\text{Tendency}} = \langle Q_{sw} \rangle - \underbrace{\left\langle \int_{-h}^{0} \rho_0 c_p \left[\nabla_h \cdot (\mathbf{u}T) + \frac{\partial (wT)}{\partial z} \right] dz \right\rangle}_{\text{HHF}\quad\text{VHF}} + \langle Q_{mix} \rangle$$

where T is the potential temperature, ρ_0 is ocean reference density, c_p is ocean specific heat capacity, $\langle \cdots \rangle$ denotes spatial average, Q_{sw} is the incoming shortwave radiation, $\mathbf{u} = (u, v)$ is horizontal velocity and w is vertical velocity, $\nabla_h = (\frac{\partial}{\partial x}, \frac{\partial}{\partial y})$, Q_{mix} is the heat flux due to horizontal and vertical mixing (including longwave and turbulent heat fluxes). HHF and VHF respectively denote horizontal heat flux and vertical heat flux. The small increase in tendency term (Fig. S3) is related to an amplified winter cooling that counteracts the strong warming tendency in summer.

2.6 Liang-Kleeman information flow

The Liang-Kleeman information flow method(Liang, 2014, 2021; Liang & Kleeman, 2005) is applied for determining the causal influences. This method is based on information flow within dynamical systems(Liang & Kleeman, 2005), allowing for assessing causal influences between timeseries. It has been widely applied in various research areas (e.g., causal influence between radiative forcings and global warming(Stips, Macias, Coughlan, Garcia-Gorriz, & Liang, 2016), long-term prediction of El Niño(Liang et al., 2021), brain causal network(Cong et al., 2023), quantum mechanics(Yi & Bose, 2022), sea surface height reconstruction(Rong & Liang, 2022)). In the field of Arctic climate change, this is a novel method that has only been applied for studying the causes of Arctic sea ice decline(Docquier, Vannitsem, Ragone, Wyser, & Liang, 2022) and variability(Docquier et al., 2024; Dörr, Årthun, Docquier, Li, & Eldevik, 2024). Since multiple variables (MHWs, SIC, incoming solar radiation and SST) are considered, we apply the multivariate causality analysis(Liang, 2021). In the calculation of causal influence between two variables, the multivariate analysis takes the influences from other variables into account, while the bivariate analysis(Liang, 2014) only considers the two variables and this could make a substantial difference(Docquier, Vannitsem, & Bellucci, 2023). The strength of causal influence is measured by the absolute rate of information flowing. For timeseries of X_j and X_i, the absolute rate of information flowing from X_j to X_i is:

$$T_{j \to i} = \frac{1}{\det C} \cdot \sum_{k=1}^{d} \Delta_{jk} C_{k,di} \cdot \frac{C_{ij}}{C_{ii}}$$

Where C is the covariance matrix, d is the number of variables, Δ_{jk} are the cofactors of C, C_{ij} is the sample covariance between X_i and X_j, C_{ii} is the sample variance of X_i, and $C_{k,di}$ is the covariance between X_k and the Euler forward difference

https://doi.org/10.5194/egusphere-2025-5296
Preprint. Discussion started: 21 December 2025

approximation of $\frac{dX_i}{dt}$. The rate of information flowing is normalized (unit: percent) following Ref. (Liang, 2021) and the magnitude is for comparing the relative importance among the causal influences. If normalized $T_{j\to i}$ is significantly different from 0, X_j is a cause of X_i. If normalized $T_{j\to i} = 0$, X_j does not cause X_i. To analyze the mechanism how the resolved MHWs induce stronger Arctic Ocean warming, the multivariate analysis is applied with monthly timeseries of MHW cumulative intensity, SIC, incoming solar radiation and SST, with the seasonal cycles and long-terms trends removed for the last three variables (This removal is because the method only works on stationary time series(Liang, 2021)).

2.7 Liang-Kleeman information flow

Linear trends are calculated by linear least-squares regression based on annual means and multiplied by 10 for the linear decadal trends, and F-test is applied for the significance test. We use melt flux instead of SIC in the statistical analysis for MHW days as only melt flux is saved as daily model output. The composite-mean difference from daily climatology to MHW day is defined as(Hayashida, Matear, & Strutton, 2020)

$$Diff = \frac{1}{D}\sum_{D}(c - c_{DC})$$

where c is the melt flux/solar radiation, D is total number of days with MHW, the subscript "DC" denotes daily climatology mean based on the days of MHW date during the 31-year moving baseline. The confidence intervals of daily composite anomaly (Fig. S7) are derived from the samples of all the MHW days, with the degrees of freedom reduced by the spatial continuity. Regarding the spatial continuity, we calculate spatial decorrelation scale(Sumata et al., 2018) of daily SST anomaly during MHW (Fig. S5a-b). The spatial decorrelation scale is defined as the maximum distance beyond which correlation decreases to 1/e. The SST anomalies are correlated at smaller scales than the decorrelation scale and uncorrelated at larger scales, and thus the spatial decorrelation scale represents the spatial scale of MHW. We use the ratio between the Arctic-mean decorrelation area and model-grid area to divide the degrees of freedom.

Significance tests for the differences in Arctic Ocean amplification between high-resolution and low-resolution model versions (Fig. 8) are carried out by t-test, with samples as area-weighted model grids where the ratio is above 1. The anomalous heat budget including 95% confidence intervals (Fig.1b and Fig. S3) is derived from 1,000 bootstrap resampling of area-mean timeseries before the calculation of two-period difference(Zhang et al., 2023). The significance test for the rate of information flowing is based on the Fisher information matrix following Ref. (Liang, 2021) (Fig. 3 and Fig. 4).

3 Results

3.1 Enhanced solar heat input

To analyze the dependence on model resolution in Arctic Ocean warming, we use model periods of equal decline in sea ice concentration (SIC) and analyze heat budget of ocean warming. We assume that despite the same long-term SIC change

https://doi.org/10.5194/egusphere-2025-5296
Preprint. Discussion started: 21 December 2025

should cause same change in incoming solar radiation, resolved MHWs could induce short-term sea ice melting and facilitate more incoming solar radiation. The periods during which the Arctic-mean SIC decreases from 50% to 30% are 1976-2045 in CESM-HR and 2025-2085 in CESM-LR. These are the longest periods for both models to have a same SIC variation as SIC starts to decline in the long term (Fig. 1a). Sea ice thickness averaged over the selected periods is 0.2 m higher in CESM-HR relative to CESM-LR, indicating stronger persistence of sea ice in CESM-HR (Bitz & Roe, 2004; Massonnet et al., 2018). The longer period in CESM-HR is related to less atmospheric warming received by sea ice in the earlier warming period. The notable difference in the actual time range is related to the resolution. High-resolution climate models generally tend to have a smaller sea ice area than low-resolution versions, which is related to higher OHT and better representation of sea surface temperature (SST) and velocities in high-resolution models(Docquier et al., 2019). However, as sea ice modelling is still subject to considerable uncertainty(Jahn, Holland, & Kay, 2024; Notz & Community, 2020; Selivanova et al., 2024), there is no systematic link between the model resolution and sea ice representation. Compared to three different observational datasets, both CESM-HR and CESM-LR correctly simulate the seasonal cycle and declining trend of SIC (Fig. S1a-b), and the magnitudes of SIC are basically within the spread of observational magnitudes, with CESM-HR and CESM-LR respectively at the lower and upper limit. CESM-HR, with resolved boundary currents, simulates the sea ice edge better, especially east of Greenland (Fig. S1c-g). CESM-LR shows more sea ice than CESM-HR, and the discrepancy is probably due to a general cold bias in CESM-LR(Chang et al., 2020).

Since the actual time ranges between the models are different, the dependence of both Arctic and global warming on climate background(Eiselt & Graversen, 2022) makes it unfeasible for the comparison in the degree of Arctic (Ocean) amplification (a ratio of Arctic warming trend to global average trend(Rantanen et al., 2022)). We analyze the difference in the contribution from incoming solar radiation to the upper Arctic Ocean warming using a heat budget analysis. We first discuss the remote influence from Ocean heat transport (OHT) on the future Arctic Ocean warming. OHT into the Arctic is known as an important driver of Arctic warming and sea ice melt(Årthun, Eldevik, Smedsrud, Skagseth, & Ingvaldsen, 2012; Aylmer, Ferreira, & Feltham, 2022; Docquier & Koenigk, 2021; Dörr, Årthun, Eldevik, & Sandø, 2024; Polyakov et al., 2017; Taylor, 2018; Tsubouchi et al., 2021), and future increases in OHT will lead to increased Arctic Ocean warming(Shu et al., 2022). Oceanic eddies contribute to the OHT. Since the eddies can be better resolved in high-resolution models, the OHT is generally larger in higher-resolution versions of climate models(Decuypère, Tremblay, & Dufour, 2022; Docquier et al., 2019). In CESM-HR compared to CESM-LR, the increase in OHT from the first to the second half of the period is 10 TW higher at 60-80°N (Fig. S2). The higher OHT across Bering Strait in CESM-HR demonstrably contributes to the stronger Arctic warming(Xu et al., 2024). Via a surface heat budget (Section 2.5), the horizontal heat transport actually increases more in CESM-HR by 2 W/m^2 (Fig. S3). However, the increase in absorbed solar radiation is larger in CESM-HR compared to the other terms by the largest magnitude, even slightly more than that of horizontal heat transport (Fig. 1b and Fig. S3). This additional absorption of solar radiation is reflected where the sea ice retreats (Fig. 1c-d) and the strongest Arctic Ocean warming occurs (Fig. S1), and it could reach 5 W/m^2 more in CESM-HR. The downward solar radiation at the surface shows a corresponding decline at the same location by around 5 W/m^2 more in CESM-HR (Fig. S4a-b). The change

https://doi.org/10.5194/egusphere-2025-5296
Preprint. Discussion started: 21 December 2025

in solar radiation through sea ice hardly differs between the models (<1 W/m^2; Fig. S4c-d). Therefore, the additional absorption of solar radiation in CESM-HR is not due to atmospheric processes (e.g., change in cloud shading) or internal changes in sea ice (e.g., sea ice thinning). Next, we show that the better-resolved MHWs in CESM-HR increase the short-term sea ice melt and thereby solar heat input, which contribute to the Arctic Ocean warming.

3.2 Arctic marine heatwaves

We define the MHWs as the extreme fluctuations in SST superimposed on the seasonal cycle and long-term warming trend (Section 2.4). The cumulative intensity, defined as an integral of SST anomalies above MHW threshold over durations of MHWs, is used for the below analysis, as a property that combines frequency and daily SST anomaly of MHW. Compared to CESM-LR, CESM-HR shows more pronounced MHWs, mostly where the SIC shows strongly decreasing trends (Fig. 2a-b). The intensity of the MHWs increases significantly with sea ice retreat, as the ocean generates more variability through contact with the atmosphere. Fig. 2c shows monthly timeseries with respect to the MHW cumulative intensity where the SIC decreases significantly. The MHW in CESM-HR has a much larger amplitude in variability. Fig. 2d shows a case of MHW respectively in CESM-HR and CESM-LR, which is selected at around the same spot and certain SIC decrease of models. Because of better resolved variability in CESM-HR, the threshold for the MHW case is higher than CESM-LR. In CESM-HR, the SST anomaly during MHW case is not only larger but also have more pronounced daily variability. The spatial decorrelation scale of SST anomaly (Section 2.7), which represents the spatial scale of MHW, is tens of km in CESM-HR and generally above 100 km in CESM-LR (Fig. S5a-b). Given the strong fluctuation in MHW intensity and the small spatial scales of MHWs, Arctic MHWs are enhanced in CESM-HR by resolving localized air-sea interactions.

The main causes of MHW formation are thought to be anthropogenic warming, sea-ice melting and solar radiation[27,45,46], but we wonder whether MHWs could further favor sea-ice melting, incoming solar radiation and long-term warming trend by forming a positive feedback that ends with the dissolution of MHWs. To ensure a causal influence from MHWs, we apply Liang-Kleeman information flow method(Liang, 2014, 2021; Liang & Kleeman, 2005) (Section 2.6) to determine the causal influences. We calculate the strength of the causal influences between the MHW cumulative intensity and SIC/incoming solar radiation/SST. Before the calculation, we first remove the seasonal cycle and the long-term trends of SIC, incoming solar radiation and SST. For CESM-HR, we find significant causal influences from SIC, incoming solar radiation, SST to MHW intensity (Fig. 3a-c). More importantly, causal influences from MHW intensity to SIC, incoming solar radiation, SST are significant, with the strength of the opposing causal influences generally not larger by far (Fig. 3d-f). This indicates a positive feedback between MHWs and Arctic Ocean warming and proves the causal influence that Arctic MHWs can increase sea-ice melt and solar heat gain, reinforcing the long-term Arctic Ocean warming. More areas in CESM-HR pass the significance tests of the causal influences than CESM-LR (Fig. 4), indicating stronger positive feedback. Note that the spatial distributions of the causal influences between SST and MHW might not correspond to those of other causal influences. This is because the SST contains the signals of anomalously high temperatures during MHWs.

https://doi.org/10.5194/egusphere-2025-5296
Preprint. Discussion started: 21 December 2025

Based on the cause-effect relationships in both models, corresponding to the stronger MHW intensity, the CESM-HR indicates a stronger impact from MHWs on sea ice melt and incoming solar radiation. The months of above-average MHW cumulative intensity are characterized by less SIC, higher melt flux and more absorbed solar radiation (Fig. S6). This is more evident in CESM-HR than CESM-LR. The cumulative sum of melt flux during all MHW days shows the largest magnitude where sea ice retreats (Fig. 5a-b). It is substantially higher in CESM-HR and accounts for a larger percentage in the total melt flux (Fig. 5c-d). The same is true for the cumulative sum of incoming solar radiation during MHWs (Fig. 6). The duration of MHW per year is close between the models, as the definition of MHW leads to specific days with MHWs (Fig. S5c-d). The higher cumulative sum of melt flux and incoming solar radiation is thus caused by the higher daily SST anomaly during MHW in CESM-HR (Fig. 2d). The composite of individual MHW days in CESM-HR (Section 2.7), compared to the background climate, indicates a positive melt-flux anomaly and a stronger solar radiation anomaly (Fig. S7). The negative anomaly of melt flux in CESM-LR is related to the fact that MHWs occur at least with parts of the open ocean. With less sea ice cover, the melt flux should be below the climate background if the temperature influence of MHWs is excluded. The negative anomaly means that the influence of the temperature anomaly cannot be greater than the influence of a lower sea ice cover on the melt flux. To summarize, the consideration of MHWs in CESM-HR, which is accompanied by the gradual retreat of sea ice in the long term, leads to more ice melt in the short term and thus to more open water areas, which increases the incoming solar radiation and intensifies the warming of the Arctic Ocean. Furthermore, short-term exposure of open water together with the anomalously high SST during MHWs could increase ocean surface heat loss(Screen, Simmonds, Deser, & Tomas, 2013). MHW-induced warming could also affect the other mechanisms that modulate Arctic amplification, and future studies are needed to uncover this aspect.

Comparing the MHWs from CESM-HR, CESM-LR and observational data (Section 2.2), the timeseries of the cumulative intensity from all three datasets are characterized by pronounced interannual variability, and the variability from the models is not in phase with the variability in the observations (Fig. 7a). For comparing the magnitudes, averages of cumulative intensity over the study periods are 8.46±5.36 °C day/year in CESM-HR and 5.61±2.81 °C day/year in CESM-LR. In comparison, the average for the observational record is 11.93±10.71 °C day/year. Therefore, both model versions underestimate the magnitude and variability of MHW cumulative intensity (Fig. 7), as a general case in current numerical models(Pilo et al., 2019). However, CESM-HR shows a higher magnitude than CESM-LR, consistent with former studies showing that the highest resolution provides the relatively best simulation(Guo et al., 2022; Pilo et al., 2019). If the Arctic MHWs are better represented, future Arctic Ocean warming would be even more pronounced than current projections using high-resolution models.

4 Discussion

Our study identifies a positive feedback between stronger MHWs and larger Arctic Ocean warming. Arctic warming causes sea ice retreat and thereby increases incoming solar radiation. MHWs would emerge and are better resolved in high-

https://doi.org/10.5194/egusphere-2025-5296
Preprint. Discussion started: 21 December 2025

resolution models, leading to episodes of stronger melting of sea ice. More short-term exposures of open ocean increase the incoming solar radiation, thereby reinforcing the Arctic Ocean warming. We find that the future solar heat input into the Arctic Ocean is higher in the high-resolution than low-resolution model. Therefore, future Arctic Ocean warming is likely to exceed current projections using low-resolution models. We further make use of the publicly available high-resolution and low-resolution versions of climate models from the High Resolution Model Intercomparison Project (HighResMIP(Haarsma et al., 2016); Section 2.3) to assess Arctic Ocean warming in terms of model resolution. The average of high-resolution versions shows stronger amplified warming trend at ocean surface (Fig. 8a-b), from historical to future warming scenario (1950-2050). The region of amplified warming is located where sea ice retreats and is mainly on the Atlantic side of the Arctic Ocean at both high and low resolutions. 5 out of 6 models show a stronger amplification of sea-surface warming in their high-resolution versions (Fig. 8c). The mean rate of amplification reaches 1.85 for the high-resolution versions and 1.68 for the low-resolution versions.

The resolved MHWs should also lead to greater ocean heat loss to the atmosphere when open water and extreme temperatures occur. There is larger upward surface heat flux in CESM-HR, which intensifies as sea ice retreats (Fig. S8). This is also reflected by the larger value of the mixing term (the sum of longwave and turbulent heat fluxes) in the ocean heat budget (Fig. S3), which compensates for the larger incoming solar radiation. Although it should reinforce the warming of the Arctic surface air, the amplification of Arctic surface air does not show a clear dependence on model resolution across HighResMIP models (not shown). Therefore, the other feedbacks(Previdi et al., 2021) inducing Arctic warming might behave differently in high-resolution models. Since Arctic amplification is not just about Arctic warming, but a ratio that divides Arctic warming trend by the global warming trend(Rantanen et al., 2022), difference in the feedbacks that influence climate sensitivity(Eiselt & Graversen, 2022) could also lead to different Arctic amplification. A systematic evaluation of contributions of feedbacks that directly affect Arctic warming (e.g., Ref.(Pithan & Mauritsen, 2014; Zhou, Leung, Xie, & Lu, 2024)) , and feedbacks on climate sensitivity (e.g., Ref.(Eiselt & Graversen, 2022)) for high- and low-resolution models would be informative.

A more general implication from our study is that the cumulative effects of short-term climate extremes can amplify long-term climate change. The high-resolution models better resolve climate extremes and are therefore key for long-term climate projections. Due to their ability to resolve eddies, high-resolution climate models are expected to bring major advances in climate science(Hewitt, Fox-Kemper, Pearson, Roberts, & Klocke, 2022). Although the eddy-induced transports can be parameterized in low-resolution models(Gent, Willebrand, McDougall, & McWilliams, 1995), the turbulent energy in the climate system cannot. For example, the eddy kinetic energy at the Arctic Ocean surface in high-resolution model is multiple times larger than in low-resolution model(Li et al., 2024). This additional turbulent energy provides stronger mixing and thus generates more intrinsic variability, which increases the probability and intensity of MHW occurrence. It is also expected that more degrees of freedom in the high-resolution models will lead to more variability in the climate systems. The resolved climate extremes in high-resolution models could cause unexpected climate transitions. Nevertheless, the roles and consequences of climate extremes are not much explored. Our high-resolution model is eddy-permitting rather than eddy-

https://doi.org/10.5194/egusphere-2025-5296
Preprint. Discussion started: 21 December 2025

resolving in the polar oceans, and thus further development of eddy-resolving models is needed for such understanding. In practice, given today's high-performance computing capacities, it is possible to take a first step towards a digital twin(Chang et al., 2020) of the polar system(Bauer, Stevens, & Hazeleger, 2021) that will truly reveal climate responses to anthropogenic greenhouse gas emissions.

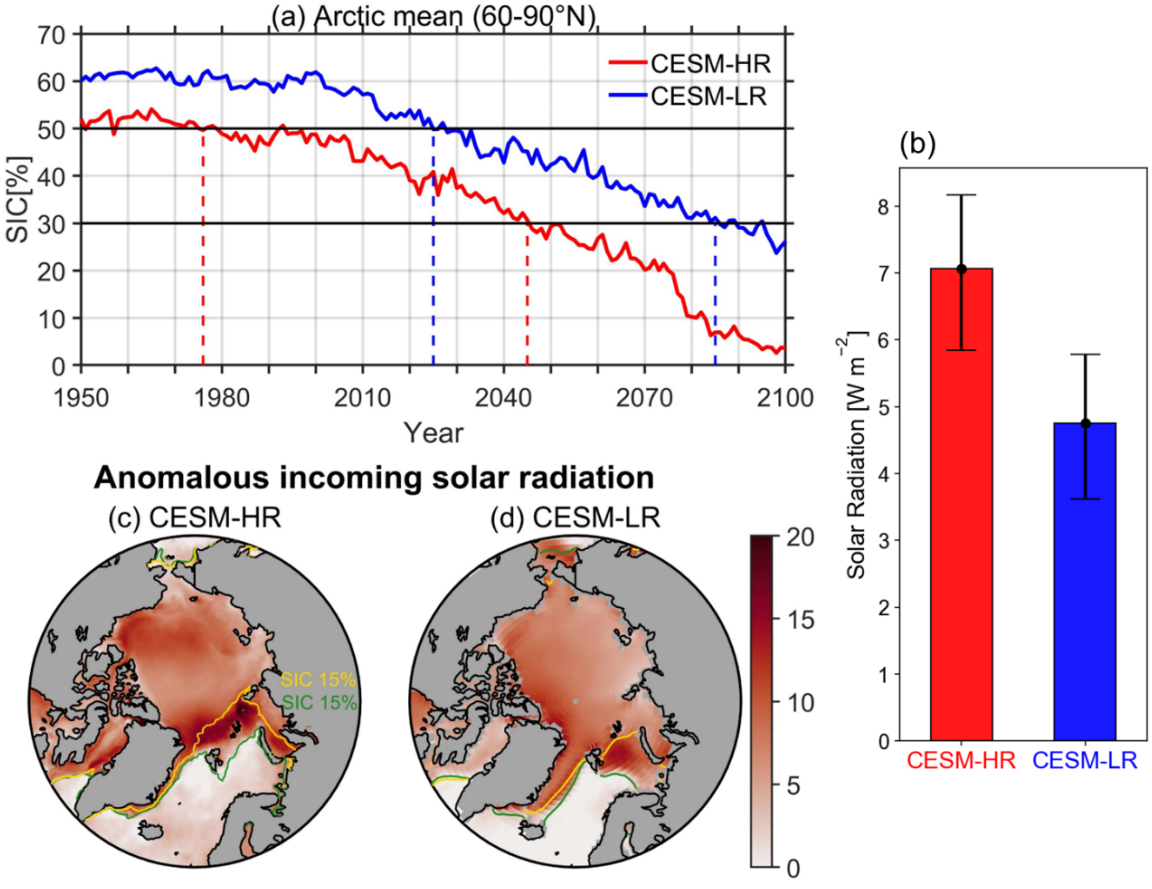

Figure 1. Increase in incoming solar radiation into the Arctic Ocean in CESM-HR and CESM-LR. A, Arctic-mean (60-90°N) SIC timeseries in CESM-HR and CESM-LR. The solid black lines indicate SIC of 50% and 30%. The red and blue dashed lines indicate the study periods in which SIC respectively in CESM-HR and CESM-LR decreases from 50% to 30%. B, anomalous incoming solar radiation in the annual area-mean ocean heat budget. "Anomalous" refers to the second-half mean minus the first-half mean of the periods. The area averaging is performed for the north of 70°N (upper 50m), where most of the Arctic sea ice is located . The error bars represent the 95% confidence intervals. C-D, spatial distributions of the anomalous incoming solar radiation in CESM-HR (C) and CESM-LR (D). Green and yellow contours in (C-D) denote 15% SIC at respectively the start and end year of the periods.

https://doi.org/10.5194/egusphere-2025-5296
Preprint. Discussion started: 21 December 2025

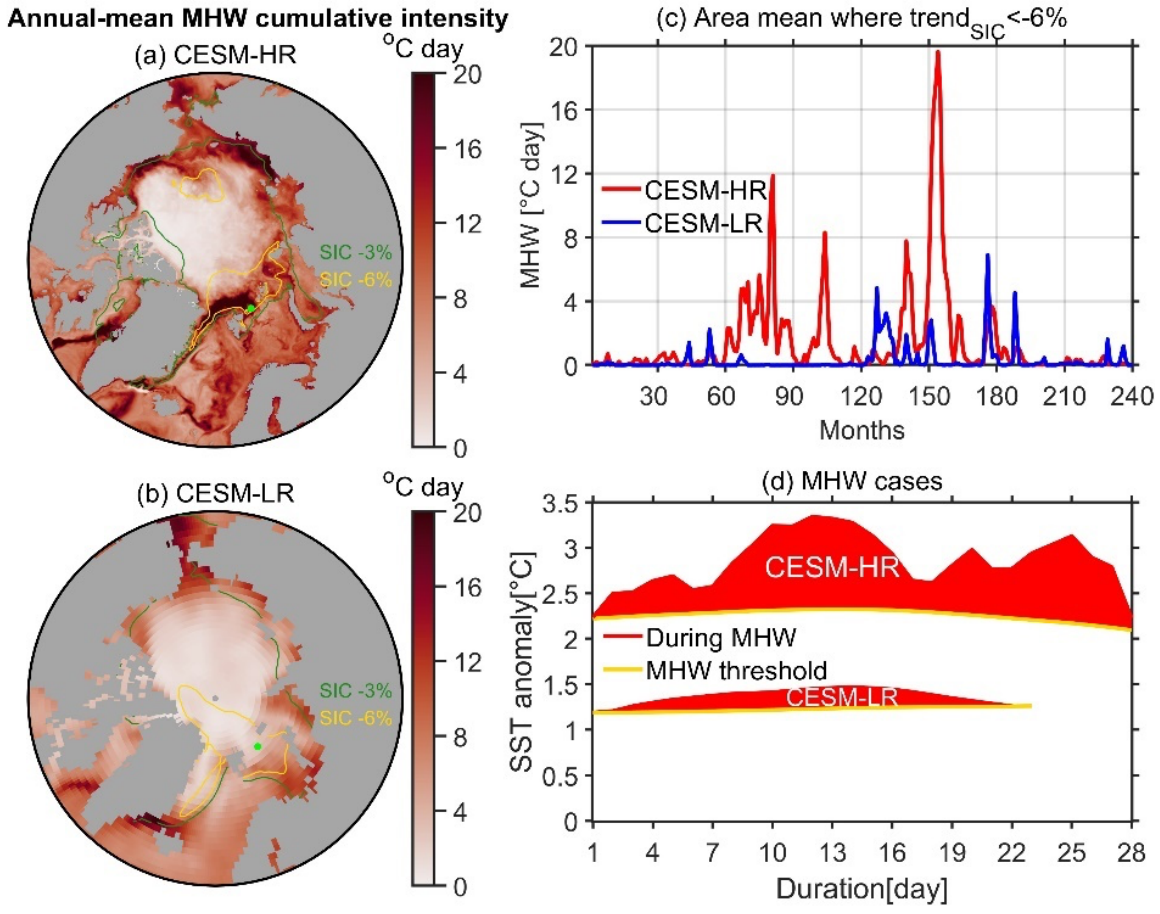

Figure 2. Arctic marine heatwaves in CESM-HR and CESM-LR. A-B, the annual-mean cumulative intensity of MHW in CESM-HR (A) and CESM-LR (B). Green and yellow contours in (A-B) denote SIC decreases by respectively 3% and 6% per decade. C, area-mean timeseries of monthly cumulative intensity. The averaged area is where the decadal trend of SIC is below -6% (A-B). The period covers the first 20 years of the study period. D, MHW cases at the grids denoted by green dots (A-B). They have the largest cumulative intensity when grid-mean SIC decreases by 20%. The SST anomaly refers to the climatology mean (mean of the 31-year moving baseline period).

https://doi.org/10.5194/egusphere-2025-5296
Preprint. Discussion started: 21 December 2025

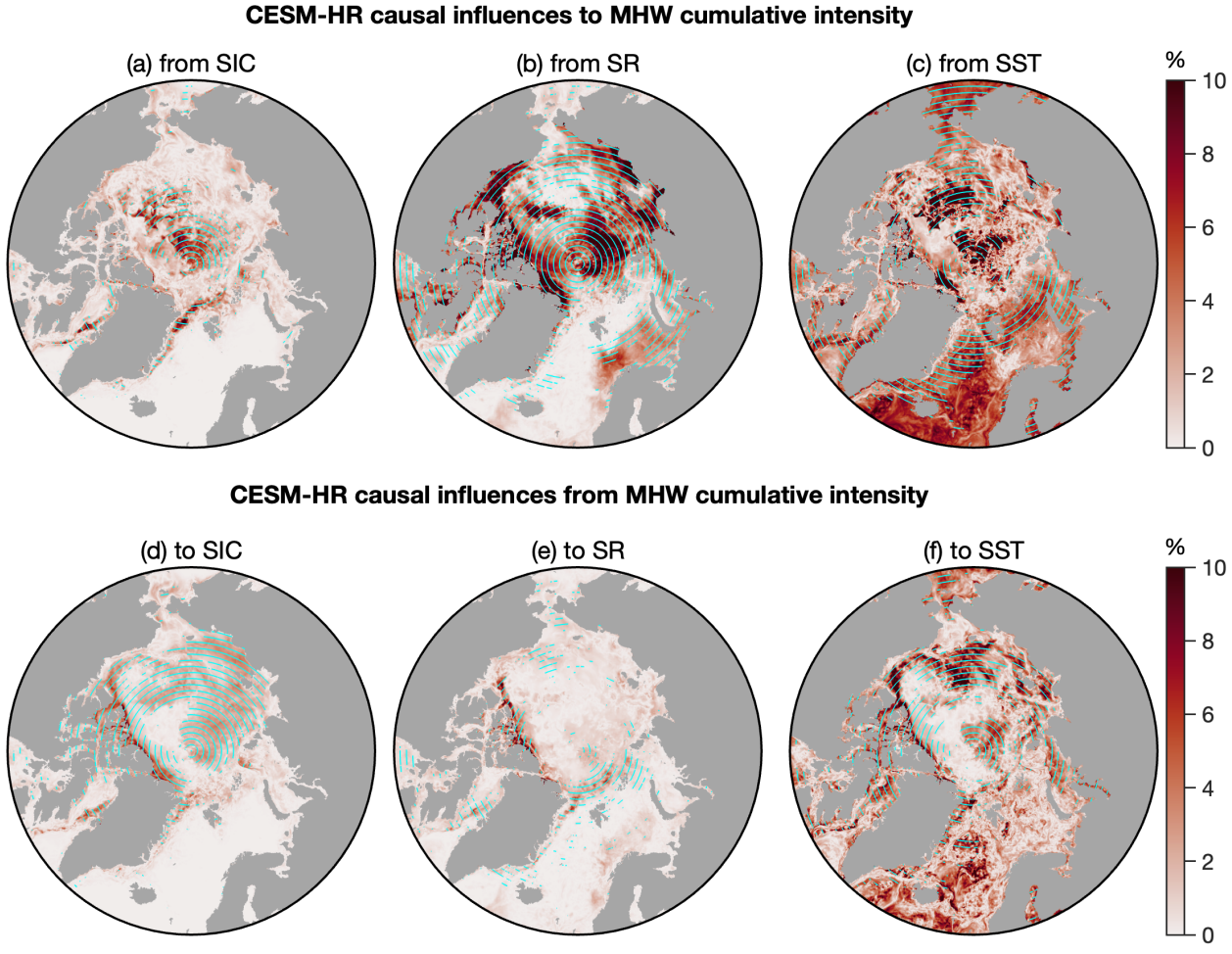

Figure 3. Causal influences between marine heatwaves and sea ice melting / incoming solar radiation / sea surface temperature in CESM-HR. A-C, the causal influences, measured by the rate of information flowing, from SIC (A), incoming solar radiation (B), SST (C) to MHW cumulative intensity. D-F, the causal influences from MHW cumulative intensity to SIC (D), incoming solar radiation (E), SST (F). The cyan lines denote where the causal influences are statistically significant at 95% confidence level. To avoid the crowdedness of grid points due to the high resolution, they are plotted with 10-point intervals on the meridional direction.

https://doi.org/10.5194/egusphere-2025-5296
Preprint. Discussion started: 21 December 2025

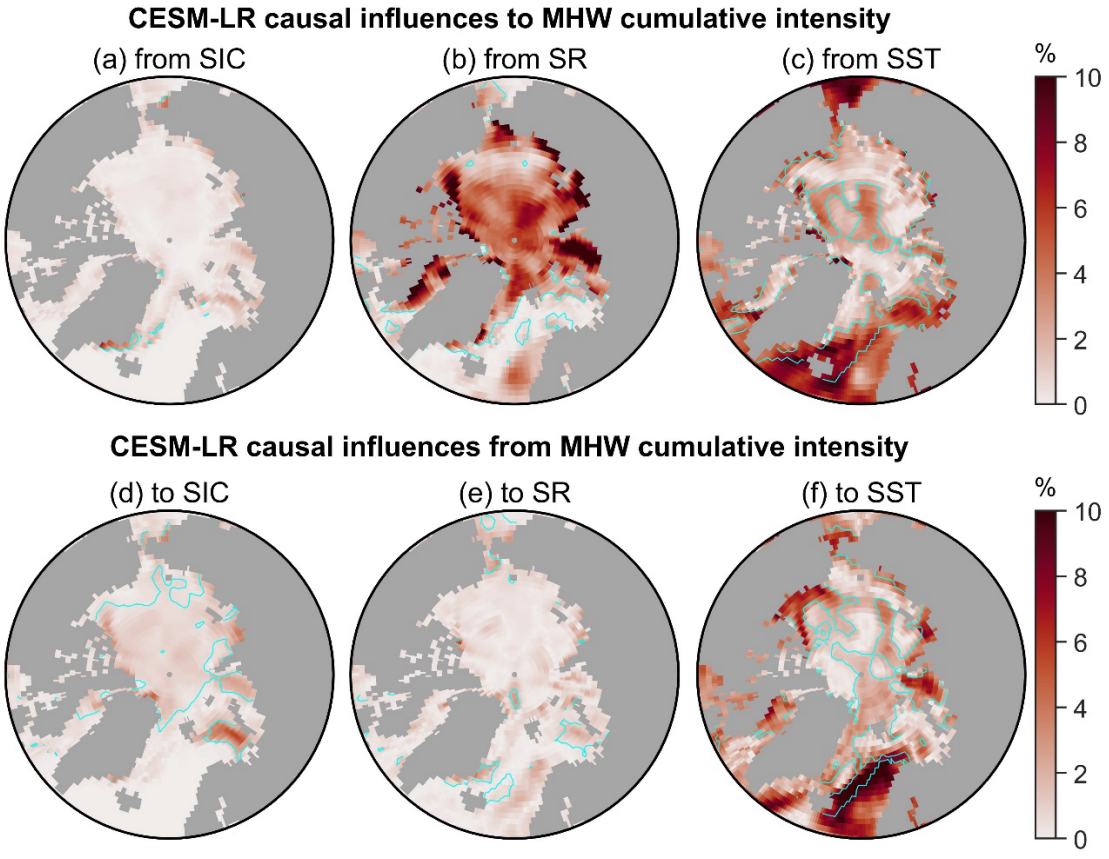

Figure 4. Causal influences between marine heatwaves and sea ice melting / incoming solar radiation / sea surface temperature in CESM-LR. a-c, the causal influences from SIC (a), incoming solar radiation (b), SST (c) to MHW cumulative intensity. d-f, the causal influences from MHW cumulative intensity to SIC (d), incoming solar radiation (e), SST (f). The cyan contourss denote where the causal influences are statistically significant at 95% confidence level.

https://doi.org/10.5194/egusphere-2025-5296
Preprint. Discussion started: 21 December 2025

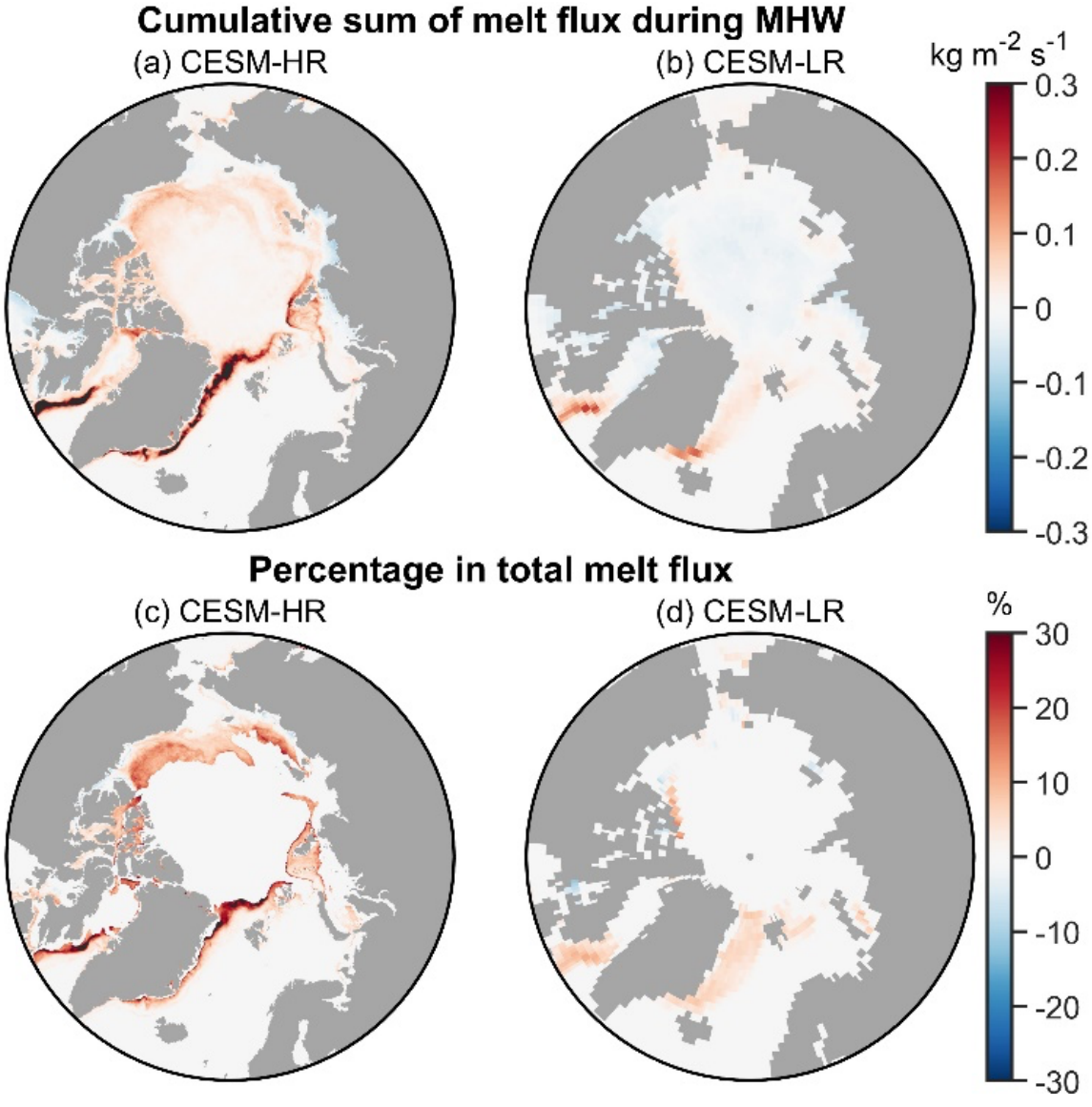

Figure 5. Cumulative melt fluxes during Arctic marine heatwaves. A-B, the cumulative sum of melt fluxes during all MHW days in CESM-HR (A) and CESM-LR (B). C-D, the percentage in total melt flux in CESM-HR (C) and CESM-LR (D). The area where the total melt flux is low (<0.3 kg m^{-2} s^{-1}) is set as 0 (C-D).

https://doi.org/10.5194/egusphere-2025-5296
Preprint. Discussion started: 21 December 2025

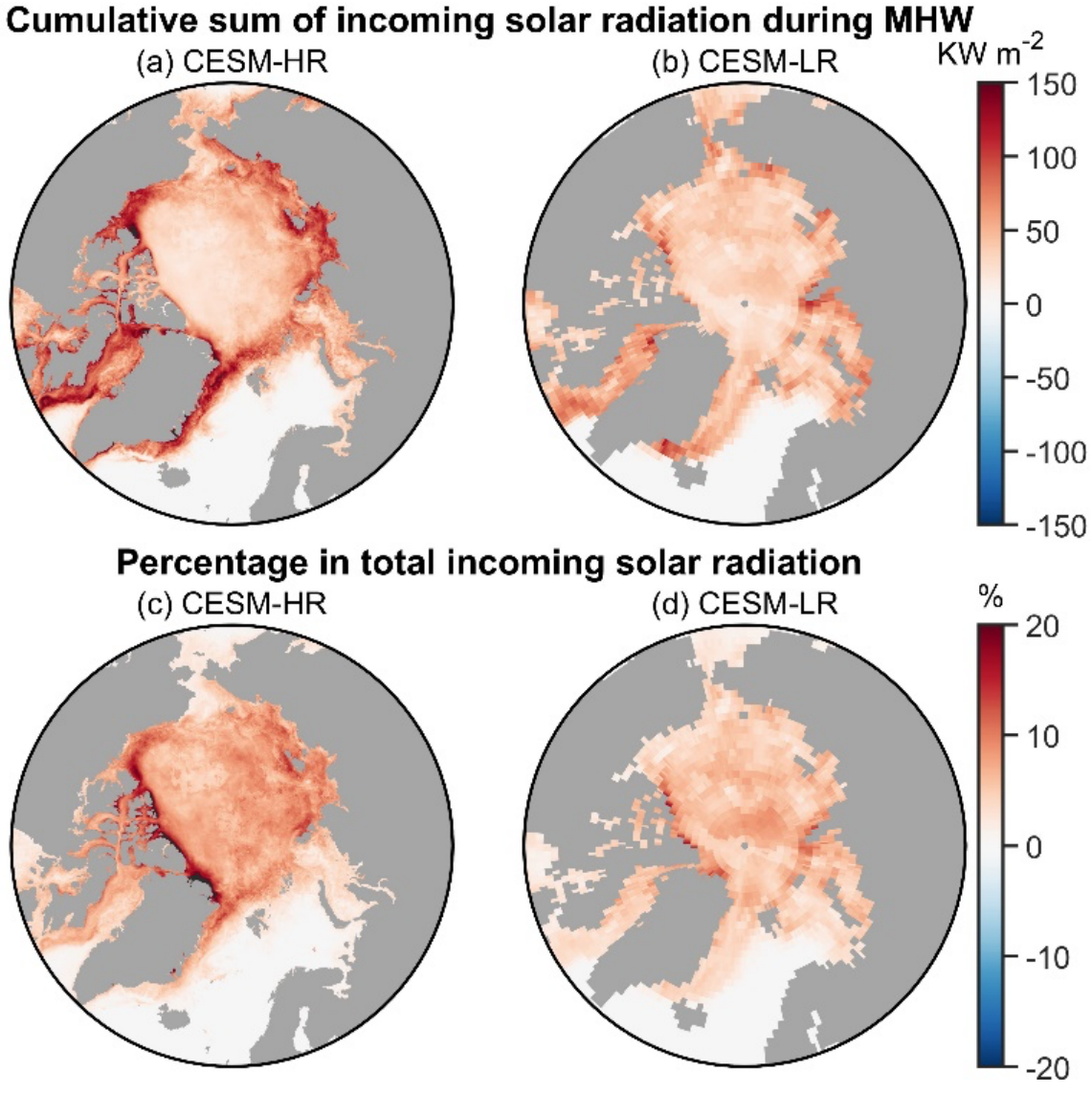

Figure 6. Cumulative incoming solar radiation during Arctic marine heatwaves. A-B, the cumulative sum of incoming solar radiation during all MHW days in CESM-HR (A) and CESM-LR (B). C-D, the percentage in total incoming solar radiation in CESM-HR (C) and CESM-LR (D).

https://doi.org/10.5194/egusphere-2025-5296
Preprint. Discussion started: 21 December 2025

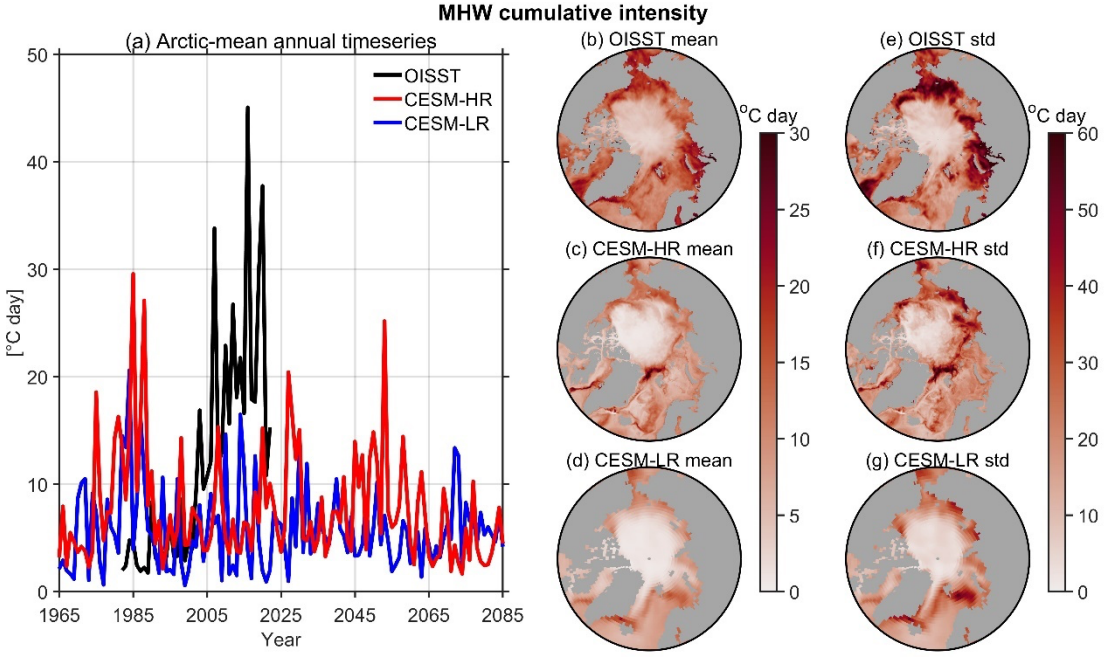

Figure 7. Comparison in the cumulative intensity of marine heatwaves between observational dataset, CESM-HR and CESM-LR. a, Arctic-mean annual cumulative intensity of MHW calculated with the observational dataset, CESM-HR and CESM-LR. b-d, annual-mean cumulative intensity based on the observational dataset (b), CESM-HR (c), CESM-LR (d). e-g, standard deviation of annual cumulative intensity based on the observational dataset (e), CESM-HR (f), CESM-LR (g). The time periods for the spatial distributions are 1982-2022 for the observational dataset and full periods of analysis (1965-2085) for the models to compare the magnitudes and variability.

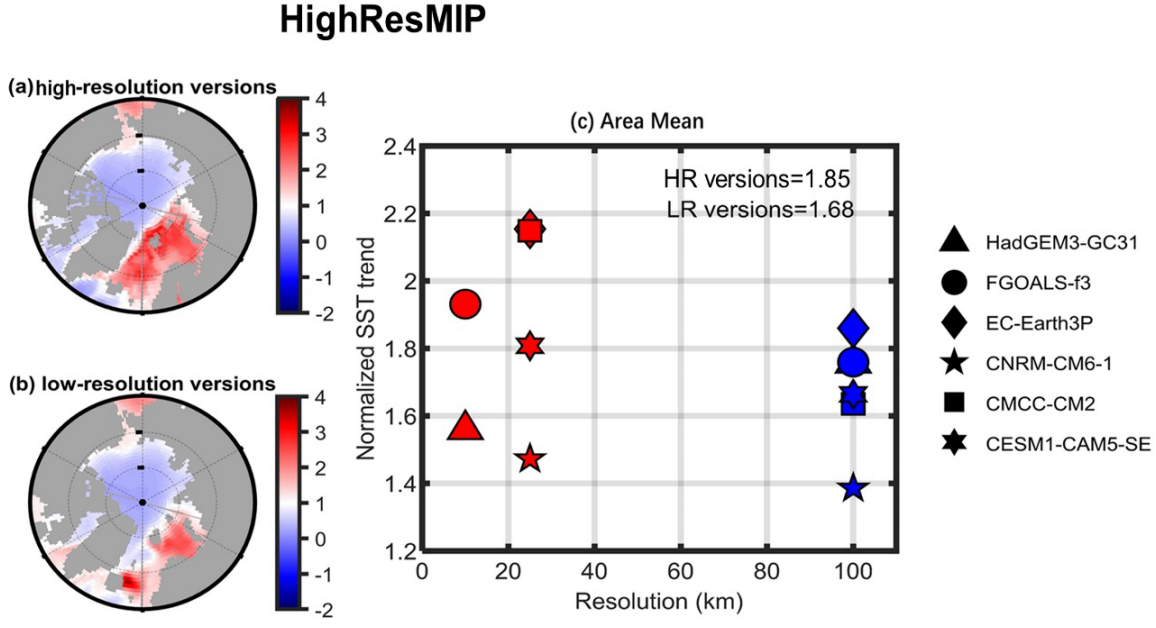

https://doi.org/10.5194/egusphere-2025-5296
Preprint. Discussion started: 21 December 2025

Figure 8. Arctic Ocean amplification in the HighResMIP models under global warming. A-B, the local trend of SST normalized by global-mean SST trend, averaged for the high-resolution versions (A) and low-resolution versions (B). C, the ratio of SST amplification averaged where above 1 (A-B) in the models. The red and blue symbols respectively denote high-resolution and low-resolution versions. The numbers denote the means for the high-resolution and low-resolution versions, respectively. For all the HighResMIP models, the differences between high-resolution and low-resolution versions at where the normalized trend is above 1 are statistically significant at 95% confidence level.

Author contribution

R.G. and G.L. proposed the central idea and drafted the manuscript. R.G., Y.D. and Y.C. performed the analysis. Q.S. and S.W. contributed to the interpretation of the results. L.W. provided with the data and computing resources and supervised the study. All authors contributed to the writing of the manuscript.

Code/Data availability

The model outputs from high-resolution and low-resolution versions of CESM are available from https://ihesp.github.io/archive/products/ds_archive/Sunway_Runs.html. The OISST dataset is available at https://psl.noaa.gov/data/gridded/data.noaa.oisst.v2.highres.html. The data of HighResMIP models can be downloaded from https://esgf-data.dkrz.de/search/cmip6-dkrz/. The observational datasets of SIC can be retrieved and downloaded from https://climexp.knmi.nl//selectfield_obs2.cgi?id=eeb887be241d13437b916d8e47749509. The CESM1.3 model code is available at Zenodo via https://doi.org/10.5281/zenodo.3637771. The calculation method of heat budget is provided by UCAR (https://pop-tools.readthedocs.io/en/latest/examples/CloseHeatBudget_POP2.html). The code for calculating the Liang-Kleeman information flow can be downloaded from https://github.com/YinengRong/LKIF.

Competing interests

Gerrit Lohmann is a member of the editorial board of Earth System Dynamics.

References

Årthun, M., Eldevik, T., Smedsrud, L. H., Skagseth, Ø., & Ingvaldsen, R. B. (2012). Quantifying the Influence of Atlantic Heat on Barents Sea Ice Variability and Retreat. *Journal of Climate, 25*(13), 4736-4743. doi:https://doi.org/10.1175/JCLI-D-11-00466.1

Aylmer, J., Ferreira, D., & Feltham, D. (2022). Different mechanisms of Arctic and Antarctic sea ice response to ocean heat transport. *Climate Dynamics, 59*(1), 315-329. doi:10.1007/s00382-021-06131-x

Bauer, P., Stevens, B., & Hazeleger, W. (2021). A digital twin of Earth for the green transition. *Nature Climate Change, 11*(2), 80-83.

Beer, E., & Eisenman, I. (2022). Revisiting the Role of the Water Vapor and Lapse Rate Feedbacks in the Arctic Amplification of Climate Change. *Journal of Climate, 35*(10), 2975-2988. doi:https://doi.org/10.1175/JCLI-D-21-0814.1

Bian, C., Jing, Z., Wang, H., Wu, L., Chen, Z., Gan, B., & Yang, H. (2023). Oceanic mesoscale eddies as crucial drivers of global marine heatwaves. *Nature Communications, 14*(1), 2970. doi:10.1038/s41467-023-38811-z

https://doi.org/10.5194/egusphere-2025-5296
Preprint. Discussion started: 21 December 2025

Bitz, C. M., & Roe, G. H. (2004). A Mechanism for the High Rate of Sea Ice Thinning in the Arctic Ocean. *Journal of Climate, 17*(18), 3623-3632. doi:https://doi.org/10.1175/1520-0442(2004)017<3623:AMFTHR>2.0.CO;2

Chang, P., Zhang, S., Danabasoglu, G., Yeager, S. G., Fu, H., Wang, H., . . . Fu, D. (2020). An unprecedented set of high-resolution earth system simulations for understanding multiscale interactions in climate variability and change. *Journal of Advances in Modeling Earth Systems, 12*(12), e2020MS002298.

Cohen, J., Screen, J. A., Furtado, J. C., Barlow, M., Whittleston, D., Coumou, D., . . . Overland, J. (2014). Recent Arctic amplification and extreme mid-latitude weather. *Nature geoscience, 7*(9), 627-637.

Cohen, J., Zhang, X., Francis, J., Jung, T., Kwok, R., Overland, J., . . . Yoon, J. (2020). Divergent consensuses on Arctic amplification influence on midlatitude severe winter weather. *Nature Climate Change, 10*(1), 20-29. doi:10.1038/s41558-019-0662-y

Cong, J., Zhuang, W., Liu, Y., Yin, S., Jia, H., Yi, C., . . . Zhang, T. (2023). Altered default mode network causal connectivity patterns in autism spectrum disorder revealed by Liang information flow analysis. *Human Brain Mapping, 44*(6), 2279-2293. doi:https://doi.org/10.1002/hbm.26209

Contzen, J., Dickhaus, T., & Lohmann, G. (2022). Variability and extremes: statistical validation of the Alfred Wegener Institute Earth System Model (AWI-ESM). *Geosci. Model Dev., 15*(4), 1803-1820. doi:10.5194/gmd-15-1803-2022

Decuypère, M., Tremblay, L. B., & Dufour, C. O. (2022). Impact of Ocean Heat Transport on Arctic Sea Ice Variability in the GFDL CM2-O Model Suite. *Journal of Geophysical Research: Oceans, 127*(3), e2021JC017762. doi:https://doi.org/10.1029/2021JC017762

Docquier, D., Grist, J. P., Roberts, M. J., Roberts, C. D., Semmler, T., Ponsoni, L., . . . Fichefet, T. (2019). Impact of model resolution on Arctic sea ice and North Atlantic Ocean heat transport. *Climate Dynamics, 53*(7), 4989-5017. doi:10.1007/s00382-019-04840-y

Docquier, D., & Koenigk, T. (2021). Observation-based selection of climate models projects Arctic ice-free summers around 2035. *Communications Earth & Environment, 2*(1), 144. doi:10.1038/s43247-021-00214-7

Docquier, D., Massonnet, F., Ragone, F., Sticker, A., Fichefet, T., & Vannitsem, S. (2024). Drivers of summer Arctic sea-ice extent at interannual time scale in CMIP6 large ensembles revealed by information flow. *Scientific Reports, 14*(1), 24236. doi:10.1038/s41598-024-76056-y

Docquier, D., Vannitsem, S., & Bellucci, A. (2023). The rate of information transfer as a measure of ocean–atmosphere interactions. *Earth Syst. Dynam., 14*(3), 577-591. doi:10.5194/esd-14-577-2023

Docquier, D., Vannitsem, S., Ragone, F., Wyser, K., & Liang, X. S. (2022). Causal Links Between Arctic Sea Ice and Its Potential Drivers Based on the Rate of Information Transfer. *Geophysical Research Letters, 49*(9), e2021GL095892. doi:https://doi.org/10.1029/2021GL095892

Dörr, J., Årthun, M., Docquier, D., Li, C., & Eldevik, T. (2024). Causal Links Between Sea-Ice Variability in the Barents-Kara Seas and Oceanic and Atmospheric Drivers. *Geophysical Research Letters, 51*(7), e2024GL108195. doi:https://doi.org/10.1029/2024GL108195

Dörr, J., Årthun, M., Eldevik, T., & Sandø, A. B. (2024). Expanding Influence of Atlantic and Pacific Ocean Heat Transport on Winter Sea-Ice Variability in a Warming Arctic. *Journal of Geophysical Research: Oceans, 129*(2), e2023JC019900. doi:https://doi.org/10.1029/2023JC019900

Eiselt, K.-U., & Graversen, R. G. (2022). Change in Climate Sensitivity and Its Dependence on the Lapse-Rate Feedback in 4 × CO2 Climate Model Experiments. *Journal of Climate, 35*(9), 2919-2932. doi:https://doi.org/10.1175/JCLI-D-21-0623.1

Frölicher, T. L., Fischer, E. M., & Gruber, N. (2018). Marine heatwaves under global warming. *Nature, 560*(7718), 360-364. doi:10.1038/s41586-018-0383-9

Gent, P. R., Willebrand, J., McDougall, T. J., & McWilliams, J. C. (1995). Parameterizing Eddy-Induced Tracer Transports in Ocean Circulation Models. *Journal of Physical Oceanography, 25*(4), 463-474. doi:https://doi.org/10.1175/1520-0485(1995)025<0463:PEITTI>2.0.CO;2

Goosse, H., Kay, J. E., Armour, K. C., Bodas-Salcedo, A., Chepfer, H., Docquier, D., . . . Vancoppenolle, M. (2018). Quantifying climate feedbacks in polar regions. *Nature Communications, 9*(1), 1919. doi:10.1038/s41467-018-04173-0

Graversen, R. G., & Wang, M. (2009). Polar amplification in a coupled climate model with locked albedo. *Climate Dynamics, 33*(5), 629-643. doi:10.1007/s00382-009-0535-6

https://doi.org/10.5194/egusphere-2025-5296
Preprint. Discussion started: 21 December 2025

Gruber, N., Boyd, P. W., Frölicher, T. L., & Vogt, M. (2021). Biogeochemical extremes and compound events in the ocean. *Nature, 600*(7889), 395-407.

Guo, X., Gao, Y., Zhang, S., Wu, L., Chang, P., Cai, W., . . . Danabasoglu, G. (2022). Threat by marine heatwaves to adaptive large marine ecosystems in an eddy-resolving model. *Nature Climate Change, 12*(2), 179-186.

Haarsma, R. J., Roberts, M. J., Vidale, P. L., Senior, C. A., Bellucci, A., Bao, Q., . . . von Storch, J. S. (2016). High Resolution Model Intercomparison Project (HighResMIP v1.0) for CMIP6. *Geosci. Model Dev., 9*(11), 4185-4208. doi:10.5194/gmd-9-4185-2016

Hayashida, H., Matear, R. J., & Strutton, P. G. (2020). Background nutrient concentration determines phytoplankton bloom response to marine heatwaves. *Global Change Biology, 26*(9), 4800-4811.

Hayashida, H., Matear, R. J., Strutton, P. G., & Zhang, X. (2020). Insights into projected changes in marine heatwaves from a high-resolution ocean circulation model. *Nature Communications, 11*(1), 4352. doi:10.1038/s41467-020-18241-x

Hewitt, H., Fox-Kemper, B., Pearson, B., Roberts, M., & Klocke, D. (2022). The small scales of the ocean may hold the key to surprises. *Nature Climate Change, 12*(6), 496-499. doi:10.1038/s41558-022-01386-6

Hobday, A. J., Alexander, L. V., Perkins, S. E., Smale, D. A., Straub, S. C., Oliver, E. C. J., . . . Wernberg, T. (2016). A hierarchical approach to defining marine heatwaves. *Progress in Oceanography, 141*, 227-238. doi:10.1016/j.pocean.2015.12.014

Holbrook, N. J., Scannell, H. A., Sen Gupta, A., Benthuysen, J. A., Feng, M., Oliver, E. C., . . . Hobday, A. J. (2019). A global assessment of marine heatwaves and their drivers. *Nature Communications, 10*(1), 2624.

Hu, S., Zhang, L., & Qian, S. (2020). Marine Heatwaves in the Arctic Region: Variation in Different Ice Covers. *Geophysical Research Letters, 47*(16), e2020GL089329. doi:https://doi.org/10.1029/2020GL089329

Jahn, A., Holland, M. M., & Kay, J. E. (2024). Projections of an ice-free Arctic Ocean. *Nature Reviews Earth & Environment, 5*(3), 164-176. doi:10.1038/s43017-023-00515-9

Li, X., Wang, Q., Danilov, S., Koldunov, N., Liu, C., Müller, V., . . . Jung, T. (2024). Eddy activity in the Arctic Ocean projected to surge in a warming world. *Nature Climate Change, 14*(2), 156-162. doi:10.1038/s41558-023-01908-w

Liang, X. S. (2014). Unraveling the cause-effect relation between time series. *Physical Review E, 90*(5), 052150. doi:10.1103/PhysRevE.90.052150

Liang, X. S. (2021). Normalized Multivariate Time Series Causality Analysis and Causal Graph Reconstruction. *Entropy, 23*(6), 679.

Liang, X. S., & Kleeman, R. (2005). Information Transfer between Dynamical System Components. *Physical Review Letters, 95*(24), 244101. doi:10.1103/PhysRevLett.95.244101

Liang, X. S., Xu, F., Rong, Y., Zhang, R., Tang, X., & Zhang, F. (2021). El Niño Modoki can be mostly predicted more than 10 years ahead of time. *Scientific Reports, 11*(1), 17860. doi:10.1038/s41598-021-97111-y

Manabe, S., & Wetherald, R. T. (1980). On the Distribution of Climate Change Resulting from an Increase in CO2 Content of the Atmosphere. *Journal of Atmospheric Sciences, 37*(1), 99-118. doi:https://doi.org/10.1175/1520-0469(1980)037<0099:OTDOCC>2.0.CO;2

Masson-Delmotte, V., Zhai, P., Pirani, A., Connors, S. L., Péan, C., Berger, S., . . . Gomis, M. (2021). Climate change 2021: the physical science basis. *Contribution of working group I to the sixth assessment report of the intergovernmental panel on climate change*, 2.

Massonnet, F., Vancoppenolle, M., Goosse, H., Docquier, D., Fichefet, T., & Blanchard-Wrigglesworth, E. (2018). Arctic sea-ice change tied to its mean state through thermodynamic processes. *Nature Climate Change, 8*(7), 599-603. doi:10.1038/s41558-018-0204-z

Meehl, G. A., Yang, D., Arblaster, J. M., Bates, S. C., Rosenbloom, N., Neale, R., . . . Danabasoglu, G. (2019). Effects of Model Resolution, Physics, and Coupling on Southern Hemisphere Storm Tracks in CESM1.3. *Geophysical Research Letters, 46*(21), 12408-12416. doi:https://doi.org/10.1029/2019GL084057

Mitchell, J. F. B., Senior, C. A., & Ingram, W. J. (1989). C02 and climate: a missing feedback? *Nature, 341*(6238), 132-134. doi:10.1038/341132a0

Morrison, A. L., Kay, J. E., Frey, W. R., Chepfer, H., & Guzman, R. (2019). Cloud Response to Arctic Sea Ice Loss and Implications for Future Feedback in the CESM1 Climate Model. *Journal of Geophysical Research: Atmospheres, 124*(2), 1003-1020. doi:https://doi.org/10.1029/2018JD029142

https://doi.org/10.5194/egusphere-2025-5296
Preprint. Discussion started: 21 December 2025

Notz, D., & Community, S. (2020). Arctic Sea Ice in CMIP6. *Geophysical Research Letters, 47*(10), e2019GL086749. doi:https://doi.org/10.1029/2019GL086749

Oliver, E. C. J., Benthuysen, J. A., Darmaraki, S., Donat, M. G., Hobday, A. J., Holbrook, N. J., . . . Sen Gupta, A. (2021). Marine Heatwaves. *Ann Rev Mar Sci, 13*, 313-342. doi:10.1146/annurev-marine-032720-095144

Pilo, G. S., Holbrook, N. J., Kiss, A. E., & Hogg, A. M. (2019). Sensitivity of marine heatwave metrics to ocean model resolution. *Geophysical Research Letters, 46*(24), 14604-14612.

Pithan, F., & Mauritsen, T. (2014). Arctic amplification dominated by temperature feedbacks in contemporary climate models. *Nature Geoscience, 7*(3), 181-184. doi:10.1038/ngeo2071

Polyakov, I. V., Alkire, M. B., Bluhm, B. A., Brown, K. A., Carmack, E. C., Chierici, M., . . . Wassmann, P. (2020). Borealization of the Arctic Ocean in Response to Anomalous Advection From Sub-Arctic Seas. *Frontiers in Marine Science, 7*. doi:10.3389/fmars.2020.00491

Polyakov, I. V., Pnyushkov, A. V., Alkire, M. B., Ashik, I. M., Baumann, T. M., Carmack, E. C., . . . Yulin, A. (2017). Greater role for Atlantic inflows on sea-ice loss in the Eurasian Basin of the Arctic Ocean. *Science, 356*(6335), 285-291. doi:doi:10.1126/science.aai8204

Previdi, M., Smith, K. L., & Polvani, L. M. (2021). Arctic amplification of climate change: a review of underlying mechanisms. *Environmental Research Letters, 16*(9). doi:10.1088/1748-9326/ac1c29

Rantanen, M., Karpechko, A. Y., Lipponen, A., Nordling, K., Hyvärinen, O., Ruosteenoja, K., . . . Laaksonen, A. (2022). The Arctic has warmed nearly four times faster than the globe since 1979. *Communications Earth & Environment, 3*(1), 168. doi:10.1038/s43247-022-00498-3

Reynolds, R. W., Smith, T. M., Liu, C., Chelton, D. B., Casey, K. S., & Schlax, M. G. (2007). Daily High-Resolution-Blended Analyses for Sea Surface Temperature. *Journal of Climate, 20*(22), 5473-5496. doi:https://doi.org/10.1175/2007JCLI1824.1

Rong, Y., & Liang, X. S. (2022). An Information Flow-Based Sea Surface Height Reconstruction Through Machine Learning. *IEEE Transactions on Geoscience and Remote Sensing, 60*, 1-9. doi:10.1109/TGRS.2022.3140398

Screen, J. A., & Simmonds, I. (2010). The central role of diminishing sea ice in recent Arctic temperature amplification. *Nature, 464*(7293), 1334-1337. doi:10.1038/nature09051

Screen, J. A., Simmonds, I., Deser, C., & Tomas, R. (2013). The Atmospheric Response to Three Decades of Observed Arctic Sea Ice Loss. *Journal of Climate, 26*(4), 1230-1248. doi:https://doi.org/10.1175/JCLI-D-12-00063.1

Selivanova, J., Iovino, D., & Cocetta, F. (2024). Past and future of the Arctic sea ice in High-Resolution Model Intercomparison Project (HighResMIP) climate models. *The Cryosphere, 18*(6), 2739-2763. doi:10.5194/tc-18-2739-2024

Serreze, M. C., Barrett, A. P., Stroeve, J. C., Kindig, D. N., & Holland, M. M. (2009). The emergence of surface-based Arctic amplification. *The Cryosphere, 3*(1), 11-19. doi:10.5194/tc-3-11-2009

Shu, Q., Wang, Q., Årthun, M., Wang, S., Song, Z., Zhang, M., & Qiao, F. (2022). Arctic Ocean Amplification in a warming climate in CMIP6 models. *Science Advances, 8*(30), eabn9755. doi:doi:10.1126/sciadv.abn9755

Stips, A., Macias, D., Coughlan, C., Garcia-Gorriz, E., & Liang, X. S. (2016). On the causal structure between CO2 and global temperature. *Scientific Reports, 6*(1), 21691. doi:10.1038/srep21691

Stuecker, M. F., Bitz, C. M., Armour, K. C., Proistosescu, C., Kang, S. M., Xie, S.-P., . . . Jin, F.-F. (2018). Polar amplification dominated by local forcing and feedbacks. *Nature Climate Change, 8*(12), 1076-1081. doi:10.1038/s41558-018-0339-y

Sumata, H., Kauker, F., Karcher, M., Rabe, B., Timmermans, M. L., Behrendt, A., . . . Kikuchi, T. (2018). Decorrelation scales for Arctic Ocean hydrography – Part I: Amerasian Basin. *Ocean Sci., 14*(1), 161-185. doi:10.5194/os-14-161-2018

Taylor, P. C. (2018). Local processes with a global reach. *Nature Climate Change, 8*(12), 1035-1036. doi:10.1038/s41558-018-0342-3

Tsubouchi, T., Våge, K., Hansen, B., Larsen, K. M. H., Østerhus, S., Johnson, C., . . . Valdimarsson, H. (2021). Increased ocean heat transport into the Nordic Seas and Arctic Ocean over the period 1993–2016. *Nature Climate Change, 11*(1), 21-26. doi:10.1038/s41558-020-00941-3

Watelet, S., Skagseth, Ø., Lien, V. S., Sagen, H., Østensen, Ø., Ivshin, V., & Beckers, J. M. (2020). A volumetric census of the Barents Sea in a changing climate. *Earth Syst. Sci. Data, 12*(4), 2447-2457. doi:10.5194/essd-12-2447-2020

https://doi.org/10.5194/egusphere-2025-5296
Preprint. Discussion started: 21 December 2025

Xu, G., Rencurrel, M. C., Chang, P., Liu, X., Danabasoglu, G., Yeager, S. G., . . . Zhang, Q. (2024). High-resolution modelling identifies the Bering Strait's role in amplified Arctic warming. *Nature Climate Change, 14*(6), 615-622. doi:10.1038/s41558-024-02008-z

Yi, B., & Bose, S. (2022). Quantum Liang Information Flow as Causation Quantifier. *Physical Review Letters, 129*(2), 020501. doi:10.1103/PhysRevLett.129.020501

Zhang, P., Chen, G., Ting, M., Ruby Leung, L., Guan, B., & Li, L. (2023). More frequent atmospheric rivers slow the seasonal recovery of Arctic sea ice. *Nature Climate Change, 13*(3), 266-273. doi:10.1038/s41558-023-01599-3

Zhou, W., Leung, L. R., Xie, S.-P., & Lu, J. (2024). An analytic theory for the degree of Arctic Amplification. *Nature Communications, 15*(1), 5060. doi:10.1038/s41467-024-48469-w